The Astrophysical Journal, 590:149–161, 2003 June 10

THE FLARING H_2O MEGAMASER AND COMPACT RADIO SOURCE IN MARKARIAN 348

A. B. Peck,[1,2] C. Henkel,[1] J. S. Ulvestad,[3] A. Brunthaler,[1] H. Falcke,[1] M. Elitzur,[4]
K. M. Menten,[1] and J. F. Gallimore[5]

Received 2002 November 24; accepted 2003 February 20

ABSTRACT

We report on single-dish monitoring and extremely high angular resolution observations of the flaring H_2O megamaser in the Seyfert 2 galaxy Mrk 348. The H_2O line is redshifted by $\sim$130 km s^{-1} with respect to the systemic velocity, is very broad, with an FWHM of 130 km s^{-1}, and has no detectable high-velocity components within 1500 km s^{-1} on either side of the strong line. Monitoring observations made with the Effelsberg 100 m telescope show that the maser varies significantly on timescales as short as 1 day and that the integrated line flux is loosely correlated with the continuum flux. Very Long Baseline Array (VLBA) observations indicate that the maser emission arises entirely from a region less than 0.25 pc in extent, located toward a continuum component thought to be associated with the receding jet. We also report on integrated flux monitoring with the VLA between 1.4 and 43 GHz, and VLBA continuum observations of the milliarcsecond scale jets at 1.7, 8, 15, and 22 GHz. These observations have allowed us to tentatively pinpoint the location of the core, and also show the ejection of a new jet component during the current radio "flare."

Subject headings: galaxies: active — galaxies: individual (Markarian 348, NGC 262) — galaxies: jets — galaxies: Seyfert — masers — radio lines: galaxies

1. INTRODUCTION

1.1. H_2O *Megamasers*

H_2O megamasers are best known as a means to probe the accretion disks in Seyfert galaxies. In the most famous source, NGC 4258, a thin, slightly warped, nearly edge-on disk orbits in Keplerian rotation around a central mass of $4 \times 10^7\ M_\odot$ (e.g., Greenhill et al. 1995; Miyoshi et al. 1995; Herrnstein et al. 1999). VLBI studies have been used to determine the size and shape of this warped molecular disk as traced by the maser spots. A few other sources show evidence of a toroidal structure, but the distribution of maser spots is not as well understood. For example, VLBI observations of megamasers seen in NGC 3079 indicate that the structure of the maser components is consistent with a parsec-scale disk but also exhibits a significant nonrotational component (Trotter et al. 1998). NGC 3079 also exhibits H I absorption toward the core (Sawada-Satoh et al. 2000; Baan & Irwin 1995), which in some cases can be a tracer of a circumnuclear torus (e.g., Peck & Taylor 2001). The NGC 4945 maser (Greenhill, Moran, & Herrnstein 1997) is tentatively interpreted to consist of a parsec-scale disk but shows some deviations in both position and velocity of the maser components from the Keplerian model.

There is evidence, however, for a distinct class of H_2O megamaser. In these sources the amplified emission is the result of an interaction between the radio jet and an encroaching molecular cloud, rather than occurring in a circumnuclear disk. The only known sources in this class were NGC 1068 (Gallimore et al. 1996) and the Circinus galaxy (Greenhill et al. 2001), which appear to have both a circumnuclear disk and maser emission arising along the edges of an ionization cone or outflow, and NGC 1052, in which the masers appear to arise along the jet and have an FWHM $\sim$90 km s^{-1} (Claussen et al. 1998). We have recently identified the fourth such source, Mrk 348, a Seyfert 2 galaxy with a low inclination angle and an exceptionally bright and highly variable nuclear radio source (Falcke et al. 2000).

1.2. *Mrk 348*

Mrk 348 (NGC 262) is a well-studied galaxy that exhibits interesting morphology at a wide range of wavelengths. This galaxy has been classified as S0/a (deVaucouleurs, deVaucouleurs, & Corwin 1976); however, recent studies by Antón et al. (2002) indicate that it is more likely between Sa+ and Sb+. It exhibits a large H I halo (Morris & Wannier 1980) that may have been produced by an interaction with a companion galaxy (NGC 266, at an angular distance of 23′; Simkin et al. 1987).

A variety of measurements of recessional velocity, both optical and radio, exist in the literature (e.g., Cruz-Gonzales et al. 1994; Richter & Huchtmeier 1991; Bottinelli et al. 1990; Mirabel & Wilson 1984; Feldman et al. 1982; Heckman, Balick, & Sullivan 1978; Koski 1976). It is possible that some of these measurements might be affected by the gas in the halo. Because the redshift of optical emission lines can be affected by local dynamics and stellar outflows in the galaxy, we adopt the recent central H I value of Bottinelli et al. (1990; $cz_{\rm hel} = 4507$ km s^{-1}) as the most likely estimate of the systemic velocity. This corresponds to a distance of 62.5 Mpc, assuming $H_0 = 75$ km s^{-1} Mpc^{-1}.

VLBI observations of Mrk 348 at 1.417 GHz by Neff & de Bruyn (1983) show a three-component radio source with a total extent of $\sim$180 mas ($\sim$50 pc). Later observations using global VLBI at 4.8 GHz (Roy et al. 1999) show two faint continuum hot spots on either side of a much brighter

[1] Max-Planck-Institut für Radioastronomie, Auf dem Hügel 69, D-53121 Bonn, Germany.
[2] Current address: Harvard-Smithsonian Center for Astrophysics, SAO/SMA Project, P.O. Box 824, Hilo, HI 96721; apeck@cfa.harvard.edu.
[3] National Radio Astronomy Observatory, P.O. Box O, Socorro, NM 87801.
[4] Department of Physics and Astronomy, University of Kentucky, Lexington, KY 40506-0055.
[5] Department of Physics, Bucknell University, Lewisburg, PA 17837.

central peak. This central component is thought to be the core, and the separation between the outer hot spots and the core is around 50 mas to the north and 120 mas to the south. The relative intensities of the two outer components are quite similar, indicating that relativistic beaming effects are probably minimal and the jet axis should be close to the plane of the sky. Ground-based observations (Simpson et al. 1996) show evidence of an ionization cone with a half-angle of $\sim 45^\circ$, which also suggests a jet axis fairly close to the plane of the sky. Very Long Baseline Array (VLBA) images at higher frequencies (Ulvestad et al. 1999) reveal a small-scale double continuum source, the axis of which is aligned with the optical [O III] emission (Capetti et al. 1996), with a position angle of -16°. Although a broad polarized Hα line with FWHM $\sim$7400 km s^{-1} (Miller & Goodrich 1990) and a strongly absorbed hard X-ray source having $N_{\rm H} = 10^{23.1}$ cm^{-2} (Warwick et al. 1989) argue for the presence of an obscured nucleus, many attempts to detect the expected obscuring torus at radio wavelengths have not been successful. Gallimore et al. (1999) searched for H I in absorption with the VLA in 1992 but did not detect any absorption toward the radio source with a 3 σ upper limit of 4 mJy, or $\tau \sim 0.014$. Taniguchi et al. (1990) did not detect any ^{12}CO($J = 1$–0) emission or absorption using the Nobeyama Radio Observatory 45 m telescope in 1989, although their upper limit of 10.4 K km s^{-1} for this source was fairly high. Barvainis & Lonsdale (1998) reported that there was no evidence for free-free absorption in the spectral energy distributions of the core component in Mrk 348 between 1.4 and 15 GHz. *Hubble Space Telescope* (Falcke, Wilson, & Simpson 1998) observations show evidence of a dust lane crossing the nucleus.

In this paper, we present the results of Effelsberg 100 m telescope monitoring of the evolution of the H_2O line flux and 22 GHz total continuum flux density (§ 3.1), VLA monitoring of the integrated continuum flux density at various frequencies (§ 3.2), observations of the milliarcsecond scale jet morphology during the course of the continuum flare (§ 3.3), and high spatial and spectral resolution VLBA imaging of the megamaser emission at one epoch in 2000 June (§ 3.4). Details of the methods used for all of these experiments are given in § 2. In § 4, we present discussions of the physical environment in the central few parsecs in this galaxy, and the conditions which give rise to megamaser emission.

2. OBSERVATIONS AND ANALYSIS

2.1. *Effelsberg Observations*

With the Effelsberg 100 m telescope,[6] data were taken at the end of 1997 and early 1998 in a position switching mode with a 22 GHz maser receiver and a back end consisting of 1024 channels and a bandwidth of 50 MHz. The recorded system temperature was $T_{\rm sys} \sim 75$ K on a T_A^* (antenna temperature corrected for atmospheric attenuation) temperature scale. Between 2000 March and 2001 August we used a new dual-channel 22 GHz HEMT receiver in a dual beam switching mode with a beam throw of 2′ and switching frequency of 1 Hz (for details, see Falcke et al. 2000). For the measurements with the HEMT receiver, pointing could be checked on Mrk 348 itself. Amplitude calibration was obtained using NGC 7027 (5.8 Jy; see Baars et al. 1977; Ott et al. 1994) as a primary calibrator and adopting the 22 GHz gain curve given by Gallimore et al. (2001). Since Mrk 348 itself could be used as a pointing source, pointing errors do not significantly affect calibration uncertainties so that we conservatively estimate that our flux densities are accurate to $\pm 10\%$ or better.

2.2. *VLA Monitoring*

The NRAO[7] Very Large Array (VLA) observations were made at six frequencies ranging from 1.4 to 43 GHz. We observed Mrk 348 on eight dates between 1998 November and 2001 July in various configurations. The source 3C 48 was used as the primary flux density calibrator, and Mrk 348 was self-calibrated and imaged with the Astronomical Image Processing System (AIPS; van Moorsel, Kemball, & Greisen 1996). The VLA images are not shown because the radio source was unresolved in all cases; only the integrated flux densities are reported here.

2.3. *VLBA Continuum Observations*

The NRAO VLBA was used to image Mrk 348 in the continuum at three epochs: 1997.10, 1998.75, and 2000.00. Observing frequencies ranged from 1.7 through 22.2 GHz, with three different frequency bands used at each epoch. The 15 GHz observations from the first two epochs have been described previously by Ulvestad et al. (1999, hereafter U99), while the remainder of the observations are reported for the first time here. In all instances, the VLBA observations utilized four 8 MHz intermediate frequency (IF) channels with two-bit sampling of the data, resulting in total data rates of 128 Mbit s^{-1}. At the first two epochs, single polarizations were observed at each frequency, while dual polarizations were used at the third epoch. Between 1 and 3 hr was spent integrating on Mrk 348 in each of the frequency bands observed at each epoch. Details of the observations are summarized in Table 1.

All data calibration was carried out in AIPS. The amplitudes of the VLBA data were calibrated by means of the standard antenna gain files maintained by VLBA staff as well as system temperatures measured every 1–2 minutes during the observations. This calibration is estimated to be accurate to $\pm 5\%$ at all frequencies through 15 GHz, and $\pm 10\%$ at 22 GHz due to the increased (variable) impact of atmospheric emission. At the first epoch, the antennae at North Liberty, Iowa and Hancock, New Hampshire were not used due to snow and ice in the dishes, while the Pie Town, New Mexico antenna failed during the second epoch. Low-elevation data (typically below 10°) were discarded at the higher frequencies; other data editing was minor. Residual clock errors were removed by means of observations of a strong calibrator source or the application of the pulse-calibration tones inserted at the VLBA front ends. Residual delay, rate, and phase errors were derived in most cases by constructing "fringe" solutions on Mrk 348 itself; however, at the first epoch, Mrk 348 was relatively low in flux, so the local phase-reference calibrator J0112+3522 was used instead. Following the initial calibration, data were self-

[6] The 100 m telescope at Effelsberg is operated by the Max-Planck-Institut für Radioastronomie (MPIfR) on behalf of the Max-Planck-Gesellschaft (MPG).

[7] The National Radio Astronomy Observatory is a facility of the National Science Foundation operated under cooperative agreement by Associated Universities, Inc.

TABLE 1
VLBA CONTINUUM OBSERVATIONS

UT Date	Frequency (GHz)	Polarization	B_{maj} (mas)	B_{min} (mas)	P.A. (deg)	rms (mJy beam^{-1})
1997.10	1.667	LCP	7.90	5.11	−24.5	0.06
1997.10	4.987	LCP	2.66	1.67	−22.0	0.08
1997.10	15.365	LCP	0.80	0.45	−15.0	0.54
1998.75	8.421	RCP	1.54	0.92	−1.5	0.10
1998.75	15.365	LCP	0.80	0.45	−15.0	1.14
1998.75	22.233	LCP	0.56	0.31	−6.9	0.63
2000.00	8.421	Dual	1.65	0.99	−3.0	0.25
2000.00	15.365	Dual	0.86	0.54	−11.1	0.50
2000.00	22.233	Dual	0.63	0.36	−10.4	0.80

calibrated and imaged in both AIPS and DIFMAP (Shepherd 1997), resulting in the final images discussed in this paper. Images made in AIPS used an intermediate weighting with a Briggs robustness parameter of 0. Gaussian fits were made to component flux densities, sizes, and relative positions. For the extended lobes seen at 1.7 GHz, flux densities were determined by integrating over the portions of the images where significant emission was detected.

2.4. *VLBA Spectral Line Observations*

The high spatial resolution observations of the maser line were made using all 10 antennae of the VLBA on 2000 June 10. Mrk 348 was observed for 9 hr over a 12 hr period. Because the line was seen in the March Effelsberg observations to be too broad to fit in a single 16 MHz IF (full width at zero power less than 250 km s^{-1}), two IFs of 16 MHz each in both right and left circular polarizations were used, overlapped somewhat in frequency. 256 channels were used in each IF, resulting in a channel spacing of 125 kHz. This corresponds to a velocity resolution of 1.74 km s^{-1}.

Amplitude calibration was derived using the antenna gain curves and measurements of system temperature as described in § 2.3. The calibrator source J0237+2848 (4C +28.07) was used as an initial fringe finder, following which delay and rate solutions were calculated using the bright, compact continuum source in Mrk 348 itself, using the AIPS task FRING with a solution interval of 3 minutes. The nearby source J0136+4651 was observed every 40 minutes to ensure adequate bandpass calibration. This setup provided enough bandwidth to cover the line and supply 20 line-free channels on the low-frequency end of the line that could be used to generate a clean "map" of Mrk 348 in DIFMAP. This model of clean components was then used to remove any amplitude offsets between the two IFs and between right and left circular polarizations. Unfortunately, no line-free channels were available on the high-frequency side of the line. Following calibration, the overlapping channels were removed and the two IFs were joined together, using the AIPS task UVGLU, to yield a single cube of 174 channels covering 23 MHz. Continuum subtraction was done in the *u, v* plane using the AIPS task UVLSF. Subsequent editing and imaging of all data was done using DIFMAP. The line spectra were then analyzed and fitted with Gaussian functions using the Groningen Image Processing System, GIPSY (van der Hulst et al. 1992).

3. RESULTS

3.1. *Effelsberg Monitoring of the* H_2O *Emission*

The initial detection of the flaring maser in Mrk 348 using the Effelsberg 100 m telescope took place in 2000 March (shown in Fig. 1, second profile; see also Falcke et al. 2000). Reanalysis of previous unpublished data on this source (shown in the top profile, Fig. 1) indicates that the maser was also present but only marginally detectable in late 1997. The H_2O maser line in Mrk 348 is extremely broad, with an FWHM of ∼130 km s^{-1}, although in many of the monitoring epochs the emission appears to consist of two lines that can be tentatively fitted with a broad Gaussian function at ∼4609 km s^{-1} with FWHM∼100 km s^{-1} and a narrower one at ∼4678 km s^{-1} with FWHM∼60 km s^{-1}. The amplitudes of each component vary significantly on very short timescales. There are no detectable high-velocity components within 1500 km s^{-1} on either side of the strong emission line (for the noise levels of the spectra, see Fig. 1; for upper limits over a wider velocity range, see Falcke et al. 2000).

Monitoring of the H_2O emission through 2000 June showed that the maser again decreased to its 1997/1998 level within 2 months, although Xanthopoulos & Richards (2001) report a value of 107 mJy on May 2 using MERLIN. Our May 2 profile indicates a peak flux of ∼16 mJy, consistent with our VLBA observations on June 10 (see § 3.4). Resumption of the monitoring program at Effelsberg in 2000 December showed little change in the line flux, although the component centered on ∼4609 km s^{-1} appears to be slightly stronger than the higher velocity feature. In 2001 February, however, another flare appears to have begun. The observations made in early 2001 April (see Fig. 1) show that the FWHM line width decreased to 60 ± 3 km s^{-1}, and the velocity centroid increased from 4642 km s^{-1} to ∼4665 ± 1 km s^{-1}. Thus, it seems that only the higher velocity line component was flaring. Following this peak near April 2, the line again began to decrease in flux. Further observations show that in 2001 June, the low-velocity component underwent a smaller flare of unknown duration. This behavior is consistent with the scenario described in § 3.4 in which the higher velocity component arises closer to the central engine of the radio source.

Figure 2 shows five spectra that were chosen to emphasize the significant variations in the line profiles over our first 16 months of observations. The first profile is the discovery spectrum, where both components had a flux of around 30 mJy. In the second profile, taken within a week of our

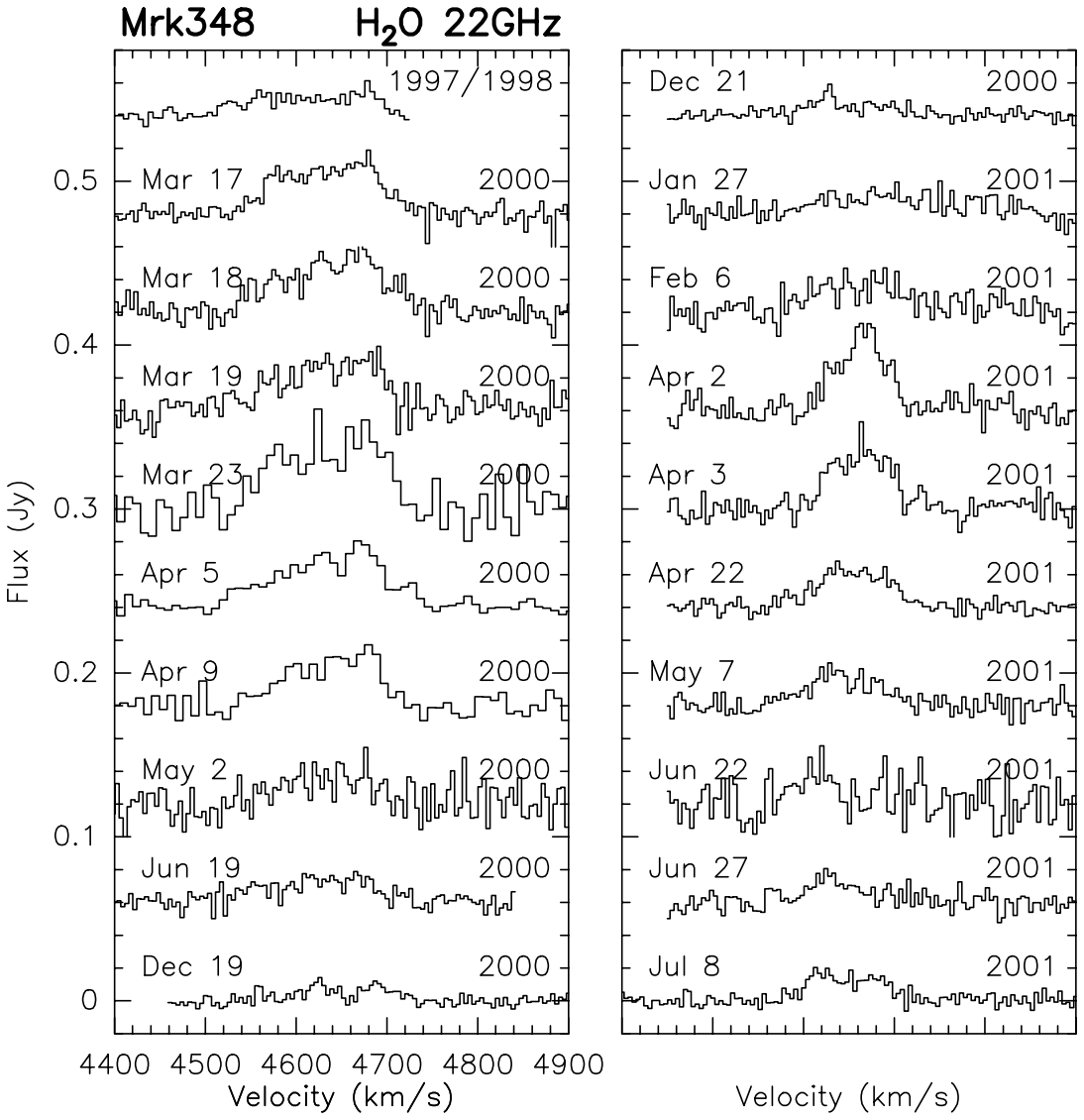

FIG. 1.—Single-dish profiles from the Effelsberg 100 m telescope. The peak flux in the line was ~40 mJy on April 9 but decreased to 9 mJy by 2000 June 19. In 2001 April, the line peak again increased to 50 mJy, but the FWHM decreased to ~65 km s^{-1}.

VLBA observations, both components verged on undetectability, and then, in the third profile, the higher velocity component flared to twice the intensity of the year previous, and the lower velocity component disappeared altogether. This change was reversed in June, shown in the fourth profile, when the lower velocity component was present, although the intensity was low, and the higher velocity component vanished. Within two weeks, both components were once again nearly equal.

Figure 3 shows the variation in line and continuum flux density with respect to time. Comparison shows that the continuum flux varies loosely with the maser flux. The implications of this for the maser position with respect to the central engine are discussed in § 4.2.

3.2. *Integrated Radio Continuum Flux Density Monitoring*

Figure 4 shows the continuum spectrum of Mrk 348 measured at eight epochs over 2.5 yr using the VLA. During the first four epochs (1998 November to 1999 March), the spectrum of Mrk 348 is inverted at centimeter wavelengths and reaches its peak at 22 GHz. During the following epochs, this turnover dropped to lower frequencies. At frequencies above the turnover, the spectrum gradually flattens with time. This behavior is similar to that in III Zw 2, where this type of evolution in turnover frequency has been linked to the expansion of synchrotron bubbles in a jet and decreasing self-absorption. This interpretation is further discussed in § 4.1.

3.3. *VLBA Continuum Imaging*

Figure 5 shows the large-scale VLBI image of Mrk 348 at 1.7 GHz, from 1997.10. The core and outer lobes shown in Figure 5 were first imaged by Neff & de Bruyn (1983); the image shown here indicates that the northern and southern lobes are quite diffuse and heavily resolved. In fact, neither lobe is detected at 5.0 GHz, with 4 σ upper limits of 0.32 mJy $beam^{-1}$. This is consistent with the scenario in which the emission in the lobes is smoothly distributed and has the spectrum of optically thin synchrotron emission. The absence of 5 GHz hot spots may indicate that there is no

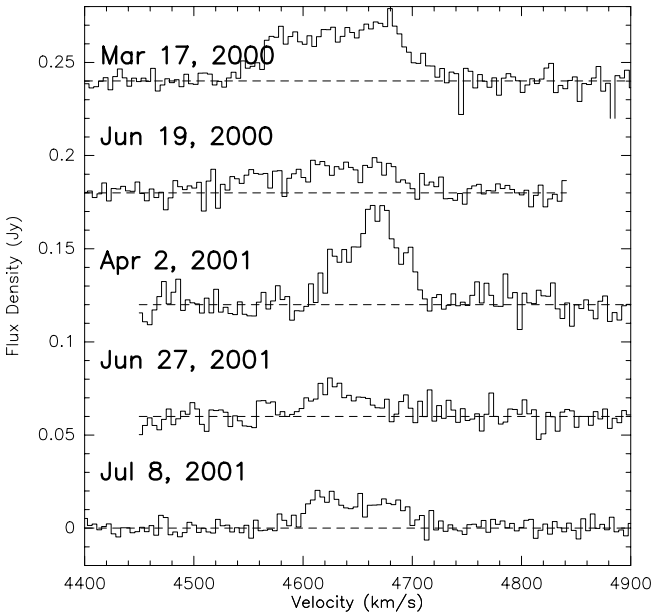

FIG. 2.—Five H_2O spectra from the Effelsberg 100 m telescope chosen to illustrate the variations in the profiles seen on timescales of days of months, as discussed in text.

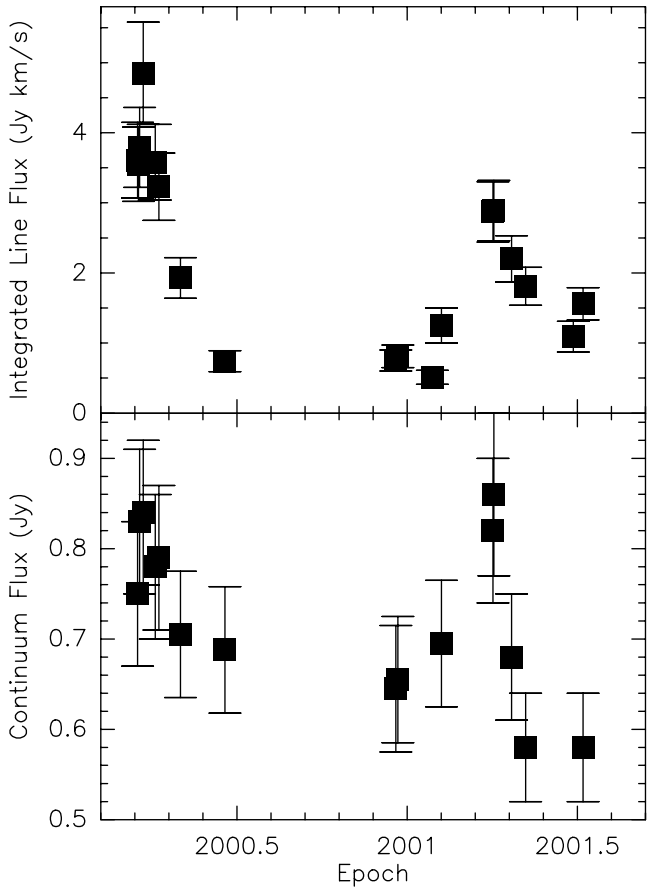

FIG. 3.—(*a*) Integrated line flux density vs. time; (*b*) continuum flux density vs. time measured with the Effelsberg 100 m telescope. The line and continuum intensity can be seen to vary concurrently. The correlation between line and continuum is $y = (-5.36 \pm 1.80) + (10.67 \pm 2.46) \times x$, where y is the integrated line flux density (Jy km s^{-1}), and x is the continuum flux density (Jy). Thus, a 1 mJy increase in continuum yields approximately 10 mJy km s^{-1} integrated line flux density.

powerful jet currently feeding the lobes. The total flux density detected in the northern lobe is 27 mJy, while that in the southern lobe is 17 mJy. These values are far below the respective 1.4 GHz values of 118 mJy and 63 mJy reported by Neff & de Bruyn (1983), who used shorter baselines in Europe, indicating that the VLBA has resolved out much of the lobe structure.

Figure 6 contains the VLBA images of the parsec-scale emission from Mrk 348 at 8, 15, and 22 GHz, from the data acquired at epoch 2000.00. In addition to the extended emission at ~1.5 mas to the north-northwest of the core, first reported by U99, the core is significantly resolved along the direction of the beam. In fact, the core appears to contain a new double source within the main peak. This component is quite obvious in the visibility function; Figure 7 shows the 22 GHz visibility amplitude and phase plotted against projected baseline along position angle 165° (15° west of north), for data from 1998.75, 2000.00, and the line-free channels from the maser observations on 2000.44. This figure shows that the dominant source (component 1 in U99) has changed from being barely resolved in 1998.75, with the flux decreasing only slightly at longer baselines, to strongly resolved in 2000.44. In the 2000.00 data, there is a clear minimum in the visibility function, which reaches almost to zero for a projected baseline separation of 210–240 million wavelengths. This implies the presence of two components with nearly equal intensity with a separation of ~0.43–0.49 mas. Multicomponent Gaussian fitting in the image plane confirms that the two strongest components are separated by 0.43 mas. A somewhat larger separation is evident from the 22 GHz continuum image made from the maser observations in 2000.44, where the peak radio emission is now significantly displaced from the southern edge of the core component. The minimum in the visibility function is at 160 million wavelengths, suggesting a separation between the two components of ~0.64 mas. This is likely to be an overestimate because the additional continuum component further to the northwest causes the visibility minimum to move toward a shorter baseline length (larger separation) than would be true for an isolated double source. This yields an upper limit on the apparent separation speed of $\beta_{\rm app} \leq 0.48$ between 2000.00 and 2000.44. The new component, which was not separately detectable at 1998.75, seems to have appeared concurrently with the flare in the nucleus of the galaxy. At 15 GHz, component 1 was reported by U99 to change from a 100 mJy unresolved component at 1997.10 to a 550 mJy resolved component at 1998.75, probably indicating the beginning of the emergence of the new component.

Table 2 contains the results of Gaussian fits to the core components at various frequencies and different epochs. Within the central few milliarcseconds of the source, components are numbered from south to north; because of the newly emerging components, component 1 of U99 has been split into first two components, 1A and 1B, for the 2000.00 data, and then a third component designated 1C that appears between them in the 2000.44 image made by averaging the line-free channels in the spectral-line data. This new component may indicate the re-emergence of the "core" component previously referred to as component 1 as 1A and 1B have separated sufficiently to "expose" 1C. Its location is marked in Figure 9.

Adding the third epoch at 15 GHz, measuring all components relative to the position of 1A, the southernmost component, we find that the proper motion of component 2

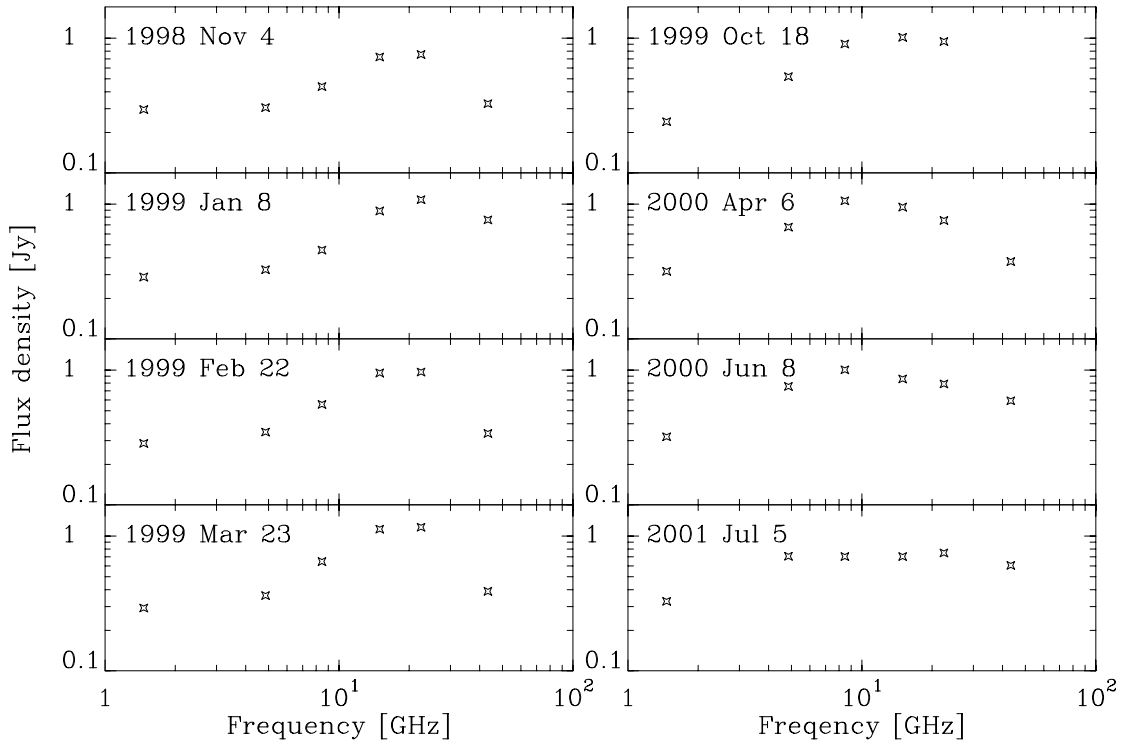

FIG. 4.—Integrated flux density measurements of Mrk 348 made with the VLA at six frequencies. The peak occurs at 22 GHz in the first four epochs, then gradually decreases in frequency over the next 20 months.

between the first and third epochs is 0.075 ± 0.004 mas yr^{-1} (1 σ error quoted), consistent with U99 who found a proper motion of 0.075 ± 0.035 mas yr^{-1} between the first two epochs. This corresponds to $\beta_{\rm app} = 0.076 \pm 0.004$. The relative speeds of components 1 (or 1A) and 2 at 8.4 and 22 GHz have not been assessed, because component 1 at 8.4 GHz is affected significantly by apparent synchrotron self-absorption, while component 2 is well resolved at 22 GHz at

TABLE 2
PARSEC-SCALE RADIO PROPERTIES

Frequency (GHz)	Component	UT Date	r[a] (mas)	P.A. (deg)	Flux Density (mJy)	Size (mas)
1.7.....	1+2+3	1997.10	0.0	...	30.6 ± 1.5	1.6×1.0, P.A. $-8°$
5.0.....	1+2+3	1997.10	0.0	...	157.3 ± 8.8	Unresolved
8.4.....	1	1998.75	0	...	228 ± 11	Unresolved
	1A	2000.00	0	...	413 ± 20	Unresolved
	1B	2000.00	0.311	-31	423 ± 21	Unresolved
	2	1998.75	1.526	-15	27.9 ± 1.4	Unresolved
	3	2000.00	2.519	-14	35.4 ± 1.8	Unresolved
15.....	1	1997.10	0	...	96 ± 5	Unresolved
	1	1998.75	0	...	552 ± 28	0.16×0.11, P.A. $-9°$
	1A	2000.00	0	...	537 ± 27	Unresolved
	1B	2000.00	0.431	-15	385 ± 19	Unresolved
	2	1997.10	1.460	-16	26 ± 2	Unresolved
	2	1998.75	1.581	-15	17 ± 1	Unresolved
	2	2000.00	1.677	-12	58 ± 3	Unresolved
	3	2000.00	2.760	-12	8 ± 1	Unresolved
22.....	1	1998.75	0	...	530 ± 27	0.15×0.11, P.A. $-22°$
	1A	2000.00	0	...	343 ± 17	Unresolved
	1B	2000.00	0.432	-15	362 ± 18	Unresolved
	1A	2000.44	0	...	40 ± 2	Unresolved
	C	2000.44	1.100	-16	299 ± 15	Unresolved
	1B	2000.44	1.473	-7.0	175 ± 9	Unresolved
	2	1998.75	1.599	-14	16 ± 1	Unresolved
	2	2000.00	1.587	-11	46 ± 2	0.9×0.2, P.A. $-9°$
	2	2000.44	1.960	-9.0	115 ± 6	Unresolved

[a] With respect to southernmost component.

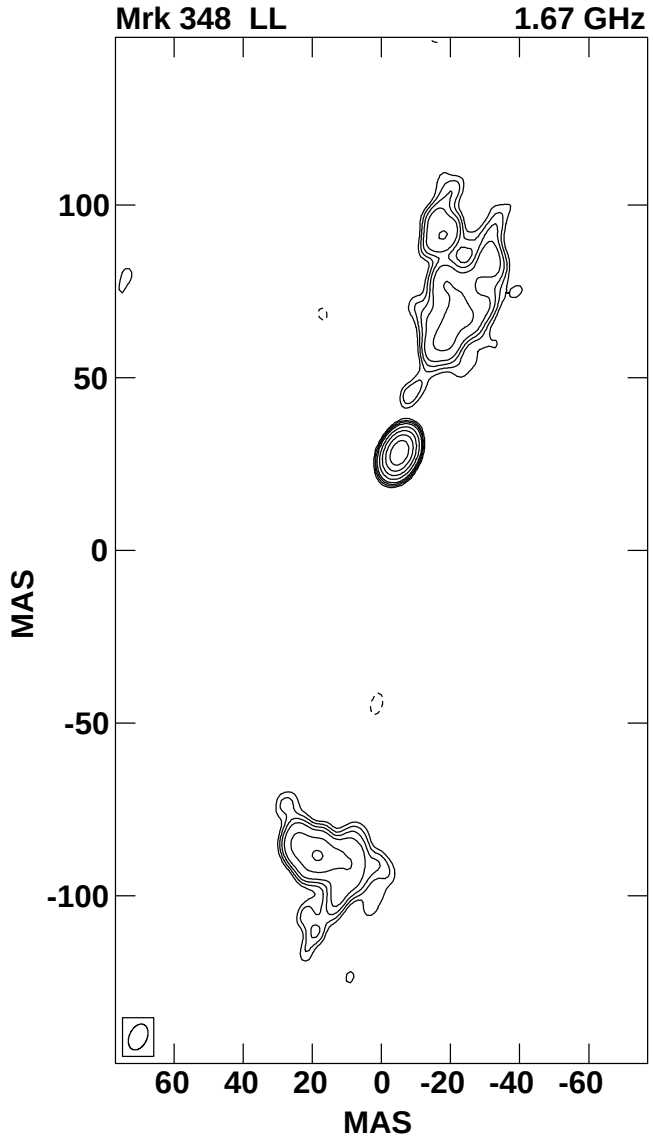

FIG. 5.—1.6 GHz VLBA image of Mrk 348, from 1997.10. The x and y axes are offsets from the phase center in milliarcseconds. Contours begin at 0.35 mJy beam^{-1}, increasing by factors of $\sqrt{2}$ to 1 mJy beam^{-1} and by factors of 2 thereafter. Negative contours are shown dashed. The peak flux density is 30 mJy beam^{-1}.

2000.0 and has no isolated component peak. We note that component 2 has brightened and component 3 has appeared at 15 GHz between 1998.75 and 2000.00, implying that they may be responding to the flare in the nucleus.

Figure 8 shows the radio spectra of components 1 (all subcomponents added together) and 2 at 1998.75 and 2000.00. The radio flare at 8.4 GHz appears to lag the flares at 15 and 22 GHz (also shown in the integrated flux measurements in Fig. 4), perhaps due to optical depth effects; in this regard, at 2000.00, component 1A is $\sim$0.12 mas closer to 1B at 8.4 GHz than at the higher frequencies. The spectrum of component 1 seems to have a maximum near 15 GHz at both epochs, and its subcomponents also peak near 15 GHz. Given the subparsec sizes of the components, synchrotron self-absorption is likely. However, since all components show a peak relatively near the same frequency at different epochs, the frequency of the peak emission of component 1 was probably between 5 and 15 GHz at 1997.10. This may imply that the radio emitters are free-free absorbed by a common parcel of foreground gas, perhaps in the circumnuclear torus that was discussed by U99.

3.4. *VLBA Spectral Line Imaging*

Figure 9 shows three line profiles toward Mrk 348 taken in 2000.44. The maser emission is clearly seen to lie along the line of sight to component 2, the fainter continuum component, rather than components 1A, 1C, and 1B, which comprise the brightest region of the continuum source. The Gaussian fit to the line shown in the upper left profile has an amplitude of 14 ± 2 mJy and an integrated flux of 2.11 ± 0.34 Jy beam^{-1} km s^{-1}, indicating that all of the flux measured in the Effelsberg May 2 observation (2.12 ± 0.18 Jy beam^{-1} km s^{-1} with a peak of 16 mJy) has been recovered. The FWHM is 139 ± 11 km s^{-1} centered on 4641 ± 2.2 km s^{-1}, consistent with the single-dish measurements and redshifted by 134 km s^{-1} with respect to the systemic velocity. A tentative two-component fit to the data yields a narrower line at 4682 ± 3 with FWHM$\sim$60 km s^{-1} and amplitude 9 ± 1 mJy, and a broader line at 4617 ± 4 with FWHM$\sim$100 km s^{-1} and amplitude 11 ± 1 mJy, again consistent with our single-dish measurements.

The plots in Figure 10 show Gaussian fits to the data at each pixel. Pixels where the signal-to-noise ratio in the line was less than 3 have been blanked. Maser emission is seen only toward the northern jet. This emission is unresolved at our angular resolution of 0.42×0.76 mas, corresponding to a linear size of less than 0.25 pc. The central panel in Figure 10 shows a velocity gradient that, in conjunction with the gradient in FWHM depicted in the right panel, appears to show that the narrower, higher velocity emission component described above arises to the southeast of the slightly broader, lower velocity line. While this gradient by itself should not be overinterpreted because the masing region is unresolved, the possibility that the higher velocity component may be caused by masing in gas closer to the central engine of the source is supported by the fact that the higher velocity component was seen to flare in 2001 April, 80 days before a similar flare in the lower velocity component was observed, as described in § 3.1. Although we do not have high enough time resolution in our monitoring program to ascertain exactly when either flare began, we can still estimate the maximum distance between the two regions responsible for these masers, based on the distance covered in 80 days at light-speed, to be 2.07×10^{17} cm, or 0.07 pc. This distance is well within the size restrictions imposed by the maximum linear size of the maser source. Much higher time resolution is needed to measure an accurate time delay.

4. DISCUSSION

Megamaser sources in which the mechanism causing population inversion is thought to be an interaction between the radio jet and a molecular cloud can provide detailed information about the conditions in the central parsecs of active galactic nuclei (AGNs). The study of these "jet masers" can yield information about the molecular clouds in the interstellar medium (ISM) of the host galaxy, because population inversion in water molecules following a shock in a molecular cloud implies a fairly narrow range of temperatures and pressures in the preshock gas (e.g., Elitzur 1995). These sources can also yield important information about

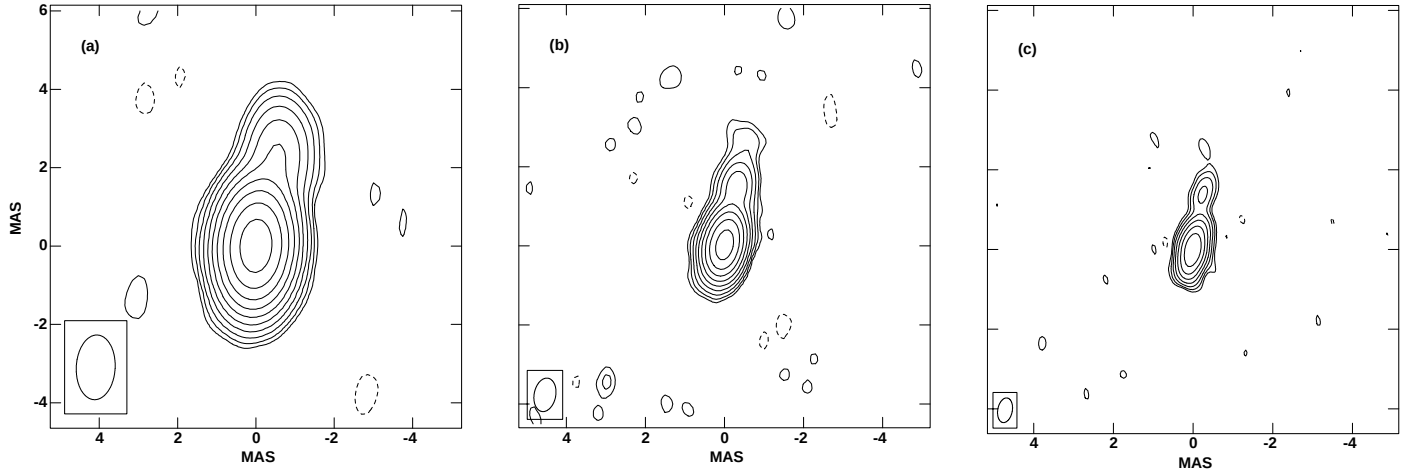

FIG. 6.—Images of Mrk 348 from 2000.00, with contour intervals increasing by factors of 2 from the lowest contour. Beam sizes, given in Table 1, are shown in the lower left corners. (*a*) Image at 8.42 GHz, with lowest contour at 1 mJy beam^{-1} and a peak of 803 mJy beam^{-1}. (*b*) Image at 15.3 GHz, with lowest contour at 2 mJy beam^{-1} and a peak of 764 mJy beam^{-1}. (*c*) Image at 22.2 GHz, with lowest contour at 4 mJy beam^{-1} and a peak of 500 mJy beam^{-1}.

the evolution of jets and their hot spots. Systematic reverberation mapping may allow us to determine jet speeds, variations in source sizes and positions, actual distances between the various targets, an estimate of inclination by comparing these distances with projected angular separations, and the relation of the maser components to continuum flares. Although we have only a small number of epochs so far, we can address the evolution of the continuum morphology on milliarcsecond scales, analyze the physical properties of the gas giving rise to maser emission, and hypothesize about future prospects of jet maser detections.

4.1. *Continuum Evolution on Milliarcsecond Scales*

VLBA observations of Mrk 348 have thus far shown only subrelativistic expansion (U99). The initially GHz-peaked integrated spectrum of Mrk 348 (Fig. 4) can be interpreted as an enhancement of one spatial region in a conical jet where the peak frequency is inversely related to the spatial scale (see Blandford & Königl 1979; Falcke & Biermann 1995). The enhancement could be caused by the formation of compact hot spots as a consequence of the jet hitting a dense target, such as a molecular cloud or torus, or the appearance of new bright components emanating from the central engine. The fact that the turnover frequency of the spectrum was dropping at the end of 1999 can be interpreted as expansion of the source and supports the interpretation of synchrotron self-absorption for the inverted spectrum. The flattening of the spectrum at higher frequencies suggests that scales even more compact and therefore probably closer to the nucleus brighten. This behavior can be compared to the spectral evolution in the recent outburst of the Seyfert 1 galaxy III Zw 2. III Zw 2 showed a self-absorbed synchrotron spectrum with a turnover frequency of 43 GHz (Falcke et al. 1999). The turnover frequency stayed constant during the outburst, and the source showed no expansion on subparsec scales. Then the spectral peak dropped quickly to 15 GHz within a few months. This phase of rapid spectral evolution in III Zw 2 was accompanied by a superluminal expansion of the source on subparsec scales (Brunthaler et al. 2000).

The evidence indicates that the center of activity in Mrk 348 is likely to be located between components 1A and 1B. At an epoch prior to 1998.75, jet components were ejected

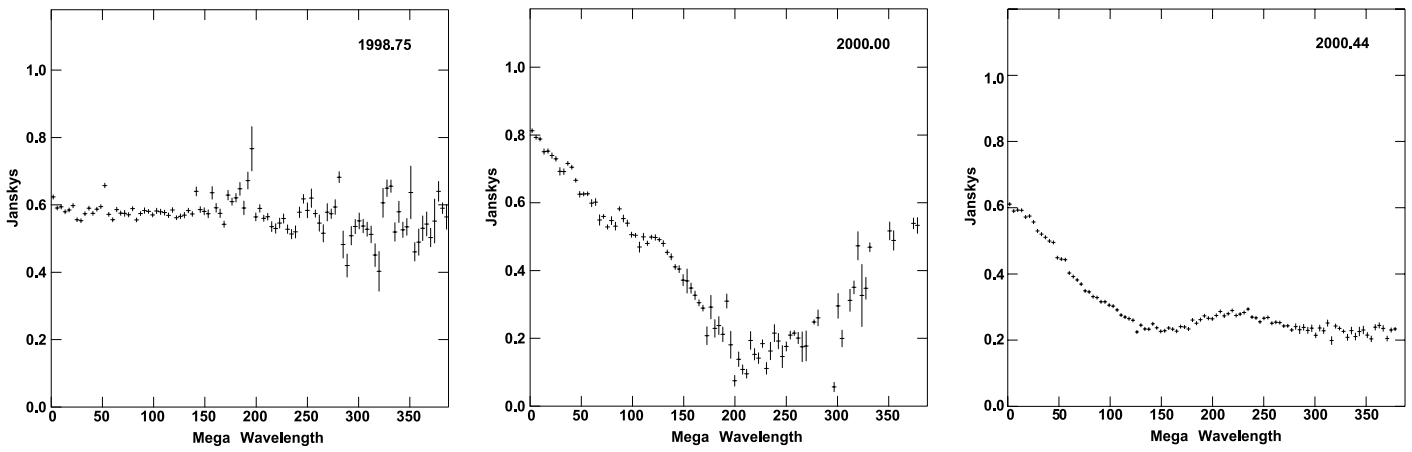

FIG. 7.—22 GHz visibility plots along position angle 165°, from epochs 1998.75 (*left panel*), 2000.00 (*center panel*), and 2000.44 (*right panel*). Note the clear minimum at a projected baseline length of 210–240 million wavelengths in 2000.00, corresponding to a nearly equal double source with a separation of 0.43–0.49 mas. There is no significant minimum in the visibilities at 1998.75.

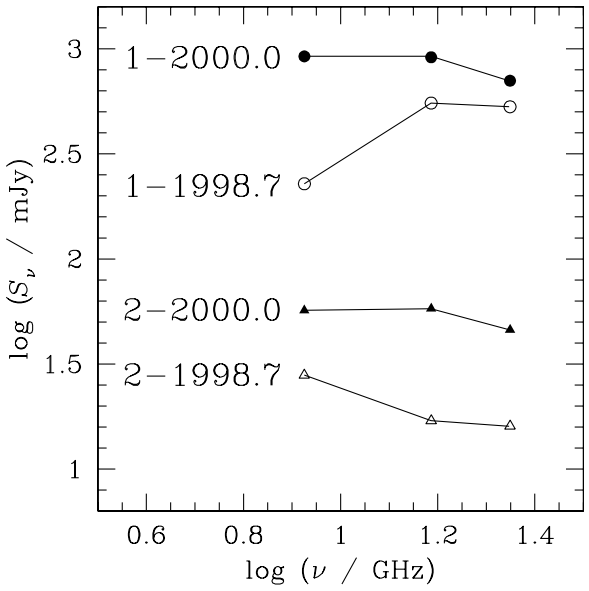

FIG. 8.—Spectra of components 1 and 2 of Mrk 348, at epochs 1998.75 and 2000.00. All subcomponents of 1 have been summed in this plot. Error bars of ±10% (including fitting errors) are slightly larger than the symbol sizes and are not shown in order to reduce clutter.

simultaneously in the approaching and receding jets, leading to both the continuum flare and the new flaring activity of the maser. We base this interpretation both on the fact that the maser emission is redshifted with respect to the systemic velocity of the source, indicating that it most likely arises in the receding jet (see § 4.3), and on the fact that we expect to see a detectable corresponding approaching jet component in any radio source where we detect a receding jet component. Thus, it seems unlikely that the central engine could be located at the southern extremity of the radio source as had been inferred by U99. Figure 9 shows the image made from 20 line-free channels at the low-frequency end of our observing band in the 2000.44 observations. Our inferred position of the core is marked with an asterisk.

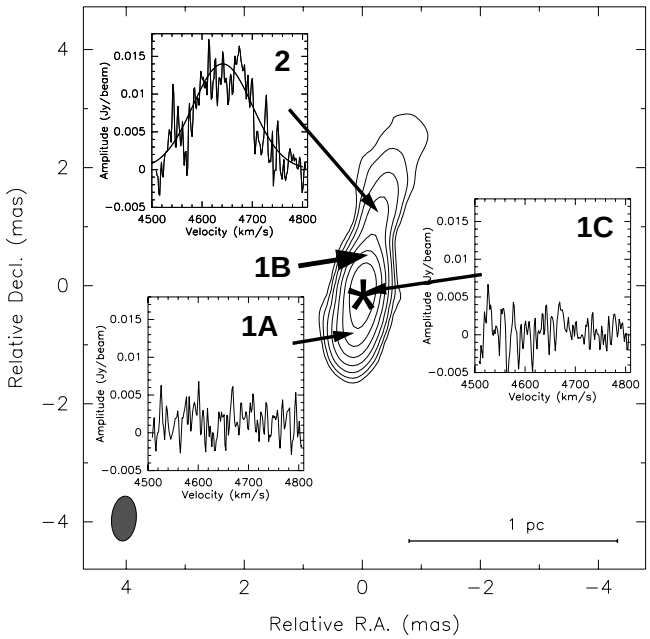

FIG. 9.—H_2O line profiles toward Mrk 348 at 21.885 GHz, superposed on the continuum map made from 20 line-free channels extracted from the low-frequency end of the observed frequency range. The data were taken in 2000.44. The RMS noise in the line profiles is ~4 mJy beam^{-1} channel^{-1}. The continuum image is naturally weighted, and the lowest contour is 5 mJy. The RMS noise in the continuum map is less than 1 mJy beam^{-1}. The suspected position of the core is indicated with an asterisk, and the other components discussed in the text are labeled accordingly.

Limits can be placed on the separation speed of the new components, 1A and 1B. A firm lower limit is derived by assuming that at least one of the new components did not exist at 1997.10, before the radio flare. Therefore, the relative separation of 0.43 mas in 2000.00 (§ 3.3) occurred in less than 2.90 yr, or at a rate of at least 0.15 mas yr^{-1}, twice the apparent speed of component 2 during the same period. An improved lower limit can be derived from the single Gaussian source size of 0.16 mas for component 1 at 1998.75. This indicates that the separation of 1A and 1B was likely to be no more than 0.16 mas at that epoch, consistent with the lack of a visibility minimum out to nearly 400 million wavelengths (Fig. 7) giving a lower limit of 0.22 mas yr^{-1} between 1998.75 and 2000.00. The resolution of component 1 at 1998.75 indicates that 1A already existed, so the upper limit to the apparent speed is 0.43 mas in 1.25 yr, or 0.34 mas yr^{-1}. Converting angular motions to linear speeds, we find $0.22 \lesssim \beta_{\rm app} \lesssim 0.34$ for the apparent relative speeds of components 1A and 1B between 1998.75 and 2000.00. This is also consistent with the upper limit of $\beta_{\rm app} \leq 0.48$ between 2000.00 and 2000.44. Although component 2 appears to have sped up between 2000.00 and 2000.44, perhaps having emerged from the far side of the molecular cloud, the apparent higher speed of 1B relative to 1A implies that it would have caught up with component 2 at approximately 2001.3. Further VLBA continuum monitoring experiments have been undertaken to determine whether this has occurred.

4.2. *Molecular Gas in the Central Few Parsecs*

One concern raised by the scenario of a molecular cloud within a projected distance on the order of 1 pc from a supermassive object is whether the gas density is high enough to keep the cloud from being disrupted by tidal forces. Using $2 \times 10^8\ M_\odot$ as the central mass of Mrk 348 (Nishiura & Taniguchi 1998), and an approximate distance of 1 pc, we can calculate whether this cloud is likely to remain intact. If we assume that the gas is roughly virialized, but infalling so that the kinetic energy is slightly less than the gravitational potential energy, then the upper limit on the circular velocity ($v_{\rm circ}$) around a central massive object of $2 \times 10^8\ M_\odot$ at a distance of 1 pc is ~900 km s^{-1}. Using this upper limit, we can then estimate the average density ($\rho_{\rm cloud}$) following the reasoning of Stark et al. (1989). They estimate the density needed to keep individual parcels of gas bound to a central cloud core near a large central potential to be $\langle \rho_{\rm cloud} \rangle \approx 3/2\pi G \times v_{\rm circ}^2 / R_0^2$ cm^{-3}, where R_0 is the distance of the cloud from the dynamical center. Using this relationship, we obtain $\langle \rho_{\rm cloud} \rangle \approx 4 \times 10^9$ cm^{-3}. This high value is regarded as an upper limit for the required density of the preshocked gas in the masing region for two reasons: first, the trajectory of the molecular cloud is not known but a stable virial orbit in a cloud this close to the central engine seems unlikely; and second, the masing region is known to be less than 0.25 pc in extent and so could correspond to a

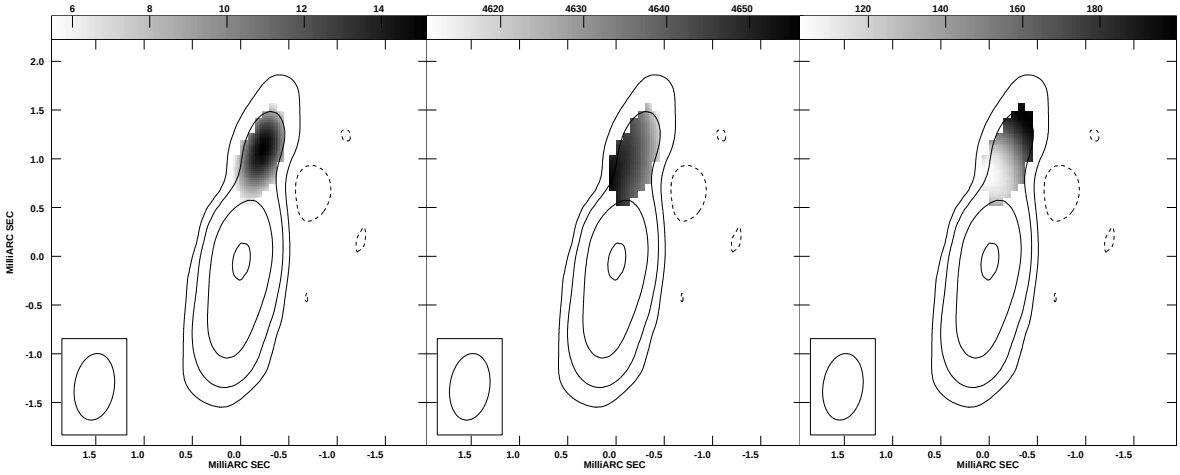

FIG. 10.—Amplitude (*left*, in mJy), velocity (*center*, in km s^{-1}) and FWHM (*right*, in km s^{-1}) fields of the maser emission obtained by fitting a Gaussian function at each pixel are shown in gray scale, superposed on the 22 GHz radio continuum image displayed as a contour plot. Although the maser emission is unresolved, the slight velocity gradient seen in the central panel, in conjunction with the gradient in FWHM, can be interpreted to mean the narrower, higher velocity line component arises closer to the central engine.

less dense region or regions in a larger molecular cloud. This upper limit is thus reasonably consistent with the highest preshock density one would expect before maser quenching sets in, around 2×10^8 cm^{-3} for high-velocity shocks (e.g., Elitzur 1995). This is also within the range of gas densities required to provide enough shielding to keep the gas in a molecular phase, as predicted by theoretical models based on NGC 4258 (Maloney 2002; Maloney, Hollenbach, & Tielens 1996). Within 1 pc of an X-ray source yielding 10^{43} ergs s^{-1}, a depth of only $\sim 10^{15}$ cm ($<10^{-3}$ pc) of shielding gas having a density of 10^7–10^8 cm^{-3} is needed, well within the size of the masing cloud estimated by the time lag between flaring components in § 3.4.

4.3. *Physical Conditions in the Masing Region*

4.3.1. *Shock Velocities and Gas Densities*

The jet in Mrk 348 is probably relativistic, but the shock velocity that gives rise to the maser emission is determined not only by the jet velocity but also by the relative densities of the jet and ambient material. The shock front is at the outer edge of an expanding bubble or cocoon driven into the cloud by the jet. A cartoon model of this scenario is shown in Figure 11. The masing region is located within or immediately behind the radiative shock. This situation is analogous to that found in high-mass star-forming regions, where collimated outflow from a young stellar object drives an overpressured cocoon into a dense ISM (see, e.g., Reid et al. 1995; Mac Low et al. 1994). The morphology of such a bubble in extragalactic sources was explored by Scheuer (1974), who determined that the bulk of the expansion would take place in the direction of jet propagation, but that the bubble would also expand laterally at slower speeds. The velocity of the shock front in the direction of propagation of the jet (v_{top}) is related to the jet velocity (v_j) and the ratio of the densities of the jet (ρ_j) and the ambient material (ρ_0) by $v_{top} = v_j(\rho_j/\rho_0)^{1/2}$ (e.g., Elitzur 1995).

In Mrk 348, the jet axis seems to be fairly close to the plane of the sky, as indicated by the optical observations of Simpson et al. (1996) and the flux densities of outer jet components (Neff & de Bruyn 1983) and also by the fact that the axis of the radio jet might be close to the plane of the galaxy, which has an inclination angle of $\sim 16^\circ$ (Braatz, Wilson, & Henkel 1997), in order for the jet to be hitting a dense molecular cloud. Further evidence for the small angle between the radio axis and the plane of the galaxy has recently been presented in the thorough study by Antón et al. (2002). The orientation of the jet close to the plane of the sky should result in shocks with the right orientation to yield strong masers along our line of sight. This situation is analogous to the Galactic masers in star-forming regions, where lower Doppler velocities are correlated with stronger masers (Elitzur, Hollenbach, & McKee 1992). Because all of the detected maser emission is redshifted with respect to the systemic velocity, we assume that the jet component toward which the maser emission is seen is probably the receding jet, and the redshift is caused by the entrainment of gas in this jet that is directed somewhere between the plane of the sky and along the line of sight away from us. In order to maintain velocity coherence, we suspect that the shock velocity in the direction of jet propagation (the "head" of

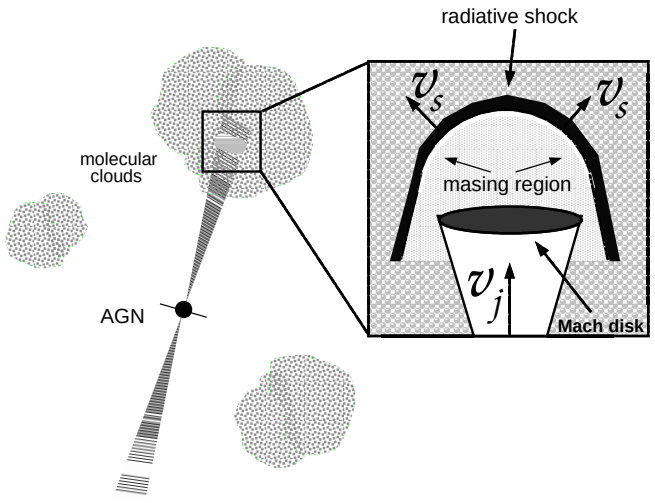

FIG. 11.—Cartoon model of the expanding bubble caused by the jet material impacting the molecular cloud. The maser emission arises within the region surrounded by the radiative shock.

the bubble) should be at least equal to the line of sight component of entrainment velocity. If the jet is close to the plane of the sky, the total shock velocity might be much higher. The maximum shock velocity expected is $\sim$300 km s^{-1}, since anything higher than that will destroy the dust grains that are required to provide condensation nuclei in the post-shock gas for the hydrogen to coalesce into H_2 and then to form H_2O (Elitzur, Hollenbach, & McKee 1989). If we assume that the maser emission comes from the head of the expanding bubble and v_j is between $0.1c$ and $0.5c$ (a range covering the measured expansion speed of the jet components), then a density contrast of 10^6 between the jet and the ambient material is required. For $\rho_0 \sim 10^8$ cm^{-3} based on the requirements described above to preserve the cloud (§ 4.2), this implies $\rho_j \sim 100$ cm^{-3}. For a higher density jet, the dust would be disrupted in the region immediately behind the shock at the head of the bubble, and so the maser emission would have to arise from regions where the shock front is expanding at slower speeds laterally into the cloud. If the two velocity components seen in the line profiles are representative of masing arising from the shocks on the "front" and "back" sides of the bubble from our viewpoint, then a lower limit on the shock velocity can be estimated on the basis of the line-of-sight components of the separation velocity. The centroids of the main line components are separated by $\sim$ 70 km s^{-1}, yielding a lower limit on the shock velocity of $\sim$35 km s^{-1}. This lower limit is still consistent with the range of velocities needed to produce population inversion in gas with a preshock density between 10^6 and a few times 10^8 cm^{-3}.

4.3.2. *Chemical Considerations*

Although few other molecules have been searched for since the onset of the continuum flare in Mrk 348, we have made a deep search for ammonia with the Effelsberg 100 m telescope. We do not detect any ammonia (NH_3) in absorption toward the continuum source, with 1 σ upper limits of between 17 and 10 mJy for the (1, 1) through (4, 4) lines with 1 km s^{-1} channel spacing (Falcke et al. 2000). This is perhaps not surprising in view of the conditions in the post-shock gas.

H_2O and NH_3 are hydrogenated molecules. These are, as a consequence of the high mobility of atomic hydrogen on cold surfaces, abundant on dust grain mantles (e.g., van Dishoeck & Blake 1998). A moderate velocity C-type shock (velocities ranging from 0 to 60 km s^{-1}), as well as a more violent J-type shock (velocities $\geq$60 km s^{-1}) that disrupts icy dust grain mantles without destroying the dust entirely, can cause a significant increase in the gas phase abundances of H_2O and NH_3. Evaporation temperatures are $\sim$100 K for both molecules.

H_2O abundances appear to be $[H_2O]/[H_2] \sim 10^{-9}$ to 10^{-7} in cool molecular cloud cores (e.g., Melnick et al. 2000; Snell et al. 2000a, 2000b, 2000c; Neufeld et al. 2000b), 10^{-6} in stellar outflow sources (e.g., Neufeld et al. 2000a), and 10^{-4} in warm shock heated gas (Melnick et al. 2000). At temperatures of several hundred to a few thousand degrees, common in C-type shocks or in the radiative region behind J-type shocks, reactions with energy barriers become efficient and direct gas phase formation of H_2O takes place via $O + H_2 \rightarrow OH + H$ and $OH + H_2 \rightarrow H_2O + H$.

In the case of NH_3, quiescent dark clouds have typically $N[NH_3]/N[H_2] \sim 10^{-7}$ (e.g., Benson & Myers 1983, their Table 5), but abundances become 10^{-6} to 10^{-5} in hot cores (e.g., Mauersberger, Henkel, & Wilson 1987; Hermsen, Wilson, & Bieging 1988; Cesaroni et al. 1994), where dust grain evaporation is believed to modify the chemical constituents of the gas. Unlike H_2O, gas phase NH_3 formation appears not to be drastically accelerated in the warm post-shock gas (e.g., Ho & Townes 1983).

H_2O is less rapidly destroyed by photodissociation than NH_3 and has a higher energy threshold for photodissociation ($\sim$6.6 vs. 4.1 eV; Crovisier 1989;[8] Suto & Lee 1983). Thus, NH_3 should be destroyed more rapidly by the ultraviolet radiation that is expected to arise during the hot adiabatic phase of a J-type shock. We thus find two qualitative scenarios: Behind a C-type shock, where the bulk of the gas remains molecular and where no additional UV-radiation is produced, H_2O *and* NH_3 abundances should be enhanced due to the release of grain mantle material into the interstellar medium. In more violent J-type shocks, however, where gas phase molecules get destroyed, H_2O reformation proceeds much faster, since potential barriers do not inhibit its direct gas-phase formation and since photodissociation by UV radiation from the shock affects predominantly NH_3. Thus, the nondetection of NH_3 implies a J-type shock scenario, consistent with the argument above that relativistic jets from the nuclei of active galaxies should have the potential to create fast J-type shocks in molecular clouds.

4.4. *Prospects for Future Maser Detections*

Although many water maser surveys have been conducted on Seyfert galaxies with low detection rates (Braatz et al. 1997 and references therein), the newly discovered "jet masers" suggest a new criterion for selecting targets for much deeper searches. In sources where the orientation of the radio jets with respect to the disks of the spiral galaxies is known, a small separation angle makes them worthy of a much longer integration than has been afforded individual sources in previous large samples. New receiver technology also makes it possible to detect much weaker masers than in the past. In particular, the masers in NGC 1052 and Mrk 348 would not have been detected but for exceptionally sensitive observations with a flat baseline (as are now routinely available at 22 GHz at the Effelsberg 100 m telescope). We are currently undertaking a survey of target sources that have been selected from a collection of Seyfert galaxies in which both the inclination of the host galaxy and the linear extent of the radio source are known (Nagar & Wilson 1999). To maximize our detection rate of jet masers, we have chosen nearby active galaxies for which there is a high probability of strong interaction between radio jets and galaxy ISM. These sources are Seyfert galaxies with a face-on ($i < 35°$) galaxy disk in optical observations and extended radio structures in VLA or VLBA observations, indicating that both the disk of the galaxy and the radio jet should be fairly close to the plane of the sky. This combination of geometries increases the probability that the radio jet lies close to the disk of the galaxy. Indeed, three of the four known jet maser sources, NGC 1068, NGC 1052, and Mrk 348 were among the galaxies selected from the parent sample using the above criteria, suggesting that this method of selection

[8] See http://wwwusr.obspm.fr/~crovisie/basemole, maintained by J. Crovisier.

should yield a much higher detection rate than has been achieved in past surveys.

5. CONCLUSIONS

During early 2000, the H_2O emission toward Mrk 348 showed a dramatic intensity increase that followed a significant increase in the flux of the nuclear radio continuum source in late 1998. The unusual line profile led us to suspect that this source, like NGC 1052 (Claussen et al. 1998), might belong to a class of megamaser galaxies in which the amplified emission is the result of an interaction between the radio jet and an encroaching molecular cloud, rather than occurring in a circumnuclear disk (Falcke et al. 2000). Analysis of our VLBA observations indicates that the maser emission does indeed arise along the line of sight to a jet component in Mrk 348, confirming this prediction. The very high line width occurring on such small spatial scales and the rapid variability indicate that the H_2O emission is more likely to arise from a shocked region at the interface between the energetic jet material and the molecular gas in the cloud where the jet is boring through, than simply as the result of amplification by molecular clouds along the line of sight to the continuum jet. The orientation of the radio jets close to the plane of the sky also results in shocks with the preferred orientation for strong masers from our vantage point. This hypothesis is supported by the spectral evolution of the continuum source, which showed an inverted radio spectrum with a peak at 22 GHz, later shifting to lower frequencies. Further evidence for the ejection of new components in the jets is shown by the subparsec scale VLBA observations made over a period of 3 yr. In this scenario, the recent high-frequency radio continuum flare, the linear motion of the brightest continuum components, and the flare in the maser emission are all attributable to the generation and ejection of new components in the approaching and receding jets. The very close temporal correlation between the flaring activity in the maser emission and the continuum flare further suggest that the masing region and the continuum hot spots are nearly equidistant from the central engine and may be different manifestations of the same dynamical events.

The gas in the molecular cloud within the central parsecs of Mrk 348 has a preshock density ranging from around 10^6 to a few times 10^9 cm^{-3}. An expanding bow-shock being driven into this cloud by the AGN jet has a velocity between 135 km s^{-1} and $0.5c$ in the direction of jet propagation, and between 35 and 300 km s^{-1} at various points along the oblique edges. This shock generates a region of very high temperature ($\leq 10^5$ K) that dissociates the molecular gas and to some extent shatters the dust grains expected to be present and/or evaporates their icy mantles. Immediately following this shock, H_2 begins forming on the surviving dust grains when the temperature has dropped to $\sim$1000 K, and this in turn provides sufficient heating to stabilize the temperature at $\sim$400 K, with gas densities of $\sim 10^8$ cm^{-3} and ultimately an H_2O abundance as high as 10^{-5}. Ammonia is not found because the levels of UV radiation remain too high, but the detection of other molecular species will help to test this scenario. For example, we are currently undertaking a search for SiO masers that might be generated as the gas is liberated from the solid phase by the shattering of dust grains toward the head of the shock. We are also searching for formaldehyde that might be located within the cocoon, and H I from the outer edges of the cloud that might be detectable in absorption toward the background continuum source.

We thank Lincoln Greenhill, James Braatz, Mark Claussen, Greg Taylor, Chris Carilli, and Floris van der Tak for enlightening discussion and/or comments. A. B. P. is grateful to Barry Clark, Peggy Perley, and the data analysts at NRAO in Socorro for prompt scheduling of and assistance with the VLBA experiment. This research has made use of the NASA/IPAC Extragalactic Database (NED), which is operated by the Jet Propulsion Laboratory, California Institute of Technology, under contract with the National Aeronautics and Space Administration.

REFERENCES

Antón, S., Thean, A. H. C., Pedlar, A., & Browne, I. W. A. 2002, MNRAS, 336, 319
Baan, W. A., & Irwin, J. A. 1995, ApJ, 446, 602
Baars, J. W. M., Genzel, R., Pauliny-Toth, I. I. K., & Witzel, A. 1977, A&A, 61, 99
Barvainis, R., & Lonsdale, C. 1998, AJ, 115, 885
Benson, P. J., & Myers, P. C. 1983, ApJ, 270, 589
Blandford, R. D., & Königl, A. 1979, ApJ, 232, 34
Bottinelli, L., Gouguenheim, L., Fouque, P., & Paturel, G. 1990, A&AS, 82, 391
Braatz, J. A., Wilson, A. S., & Henkel, C. 1997, ApJS, 110, 321
Brunthaler, A., et al. 2000, A&A, 357, L45
Capetti, A., Axon, D. J., Macchetto, F., Sparks, W. B., & Boksenberg, A. 1996, ApJ, 469, 554
Cesaroni, R., Churchwell, E., Hofner, P., Walmsley, C. M., & Kurtz, S. 1994, A&A, 288, 903
Claussen, M. J., Diamond, P. J., Braatz, J. A., Wilson, A. S., & Henkel, C. 1998, ApJ, 500, L129
Crovisier, J. 1989, A&A, 213, 459
Cruz-Gonzalez, I., Carrasco, L., Serrano, A., Guichard, J., Dultzin-Hacyan, D., & Bisiacchi, G. F. 1994, ApJS, 94, 47
de Vaucouleurs, G., de Vaucouleurs, A., & Corwin, J. R. 1976, The Second Reference Catalog of Bright Galaxies (Austin: Univ. Texas Press)
Elitzur, M. 1995, Rev. Mexicana Astron. Astrofis., 1, 85
Elitzur, M., Hollenbach, D. J., & McKee, C. F. 1989, ApJ, 346, 983
———. 1992, ApJ, 394, 221
Falcke, H., & Biermann, P. L. 1995, A&A, 293, 665
Falcke, H., Henkel, C., Peck, A. B., Hagiwara, Y., Prieto, M. A., & Gallimore, J. F. 2000, A&A, 358, L17
Falcke, H., Wilson, A. S., & Simpson, C. 1998, ApJ, 502, 199
Falcke, H., et al. 1999, ApJ, 514, L17
Feldman, F. R., Weedman, D. W., Balzano, V. A., & Ramsey, L. W. 1982, ApJ, 256, 427
Gallimore, J. F., Baum, S. A., O'Dea, C. P., Brinks, E., & Pedlar, A. 1996, ApJ, 462, 740
Gallimore, J. F., Baum, S. A., O'Dea, C. P., Pedlar, A., & Brinks, E. 1999, ApJ, 524, 684
Gallimore, J. F., Henkel, C., Baum, S. A., Glass, I. S., Claussen, M. J., Prieto, M. A., & von Kap-herr, A. 2001, ApJ, 556, 694
Greenhill, L. J., Jiang, D. R., Moran, J. M., Reid, M. J., Lo, K. Y., & Claussen, M. J. 1995, ApJ, 440, 619
Greenhill, L. J., Moran, J. M., & Herrnstein, J. R. 1997, ApJ, 481, L23
Greenhill, L. J., et al. 2003, ApJ, 590, 162
Heckman, T. M., Balick, B., & Sullivan, W. T. 1978, ApJ, 224, 745
Hermsen, W., Wilson, T. L., & Bieging, J. H. 1988, A&A, 201, 276
Herrnstein, J. R., et al. 1999, Nature, 400, 539
Ho, P. T. P., & Townes, C. H. 1983, ARA&A, 21, 239
Koski, A. T. 1976, Ph.D. thesis, Univ. California–Santa Cruz
Mac Low, M.-M., Elitzur, M., Stone, J. M., & Königl, A. 1994, ApJ, 427, 914
Maloney, P. R. 2002, Publ. Astron. Soc. Australia, 19, 88
Maloney, P. R., Hollenbach, D. J., & Tielens, A. G. G. M. 1996, ApJ, 466, 561
Mauersberger, R., Henkel, C., & Wilson, T. L. 1987, A&A, 173, 352
Melnick, G. J. et al. 2000, ApJ, 539, L87
Miller, J. S., & Goodrich, R. W. 1990, ApJ, 355, 456
Mirabel, I. F., & Wilson, A. S. 1984, ApJ, 277, 92
Miyoshi, M., Moran, J., Herrnstein, J., Greenhill, L., Nakai, N., Diamond, P., & Inoue, M. 1995, Nature, 373, 127
Morris, M., & Wannier, P. G. 1980, ApJ, 238, L7
Nagar, N. M., & Wilson, A. S. 1999, ApJ, 516, 97
Neff, S. G., & de Bruyn, A. G. 1983, A&A, 128, 318

Neufeld, D. A. et al. 2000a, ApJ, 539, L107
———. 2000b, ApJ, 539, L111
Nishiura, S., & Taniguchi, Y. 1998, ApJ, 499, 134
Ott, M., Witzel, A., Quirrenbach, A., Krichbaum, T. P., Standke, K. J., Schalinski, C. J., & Hummel, C. A. 1994, A&A, 284, 331
Peck, A. B., & Taylor, G. B. 2001, ApJ, 554, L147
Reid, M. J., Argon, A. L., Masson, C. R., Menten, K. M., & Moran, J. M. 1995, ApJ, 443, 238
Richter, O. G., & Huchtmeier, W. K. 1991, A&AS, 87, 425
Roy, A. L., et al. 1999, in Perspectives on Radio Astronomy: Science with Large Antenna Arrays, ed. M. P. van Haarlem (Dwingeloo: NFRA), 173
Sawada-Satoh, S., Inoue, M., Shibata, K. M., Kameno, S., Migenes, V., Nakai, N., & Diamond, P. J. 2000, PASJ, 52, 421
Scheuer, P. A. G. 1974, MNRAS, 166, 513
Shepherd, M. C. 1997, in ASP Conf Ser. 125, Astronomical Data Analysis Software and Systems VI, ed. G. Hunt & H. Payne (San Francisco: ASP), 77
Simkin, S. M, Su, H.-J., van Gorkom, J., & Hibbard, J. 1987, Science, 235, 1367
Simpson, C., Mulchaey, J. S., Wilson, A. S., Ward, M. J., & Alonso-Herrero, A. 1996, ApJ, 457, L19
Snell, R. L. et al. 2000a, ApJ, 539, L93
Snell, R. L. et al. 2000b, ApJ, 539, L97
———. 2000c, ApJ, 539, L101
Stark, A. A., Bally, J., Wilson, R. W., & Pound, M. W. 1989, in The Center of the Galaxy: Proc. 136th Symp. of the International Astronomical Union, ed. M. Morris (Dordrecht: Kluwer), 129
Suto, M., & Lee, L. C. 1983, J. Chem. Phys., 78, 4515
Taniguchi, Y., Kameya, O., Nakai, N., & Kawara, K. 1990, ApJ, 358, 132
Trotter, A. S., Greenhill, L. J., Moran, J. M., Reid, M. J., Irwin, J. A., & Lo, K.-Y. 1998, ApJ, 495, 740
Ulvestad, J. S., Wrobel, J. M., Roy, A. L., Wilson, A. S., Falcke, H., & Krichbaum, T. P. 1999, ApJ, 517, L81 (U99)
van der Hulst, J. M., Terlouw, J. P., Begeman, K. G., Zwitser, W., & Roelfsma, P. R. 1992, in ASP Conf. Ser. 25, Astronomical Data Analysis Software and Systems I, ed. D. M. Worral, C. Biemesderger, & J. Barnes (San Francisco: ASP), 131
van Dishoeck, E. F., & Blake, G. A. 1998, ARA&A, 36, 317
van Moorsel, G., Kemball, A., & Greisen, E. 1996, in ASP Conf Ser. 101, Astronomical Data Analysis Software and Systems V, ed. G. H. Jacoby & J. Barnes (San Francisco: ASP), 37
Warwick, R. S., Koyama, K., Inoue, H., Takano, S., Awaki, H., & Hoshi, R. 1989, PASJ, 41, 739
Xanthopoulos, E., & Richards, A. M. S. 2001, MNRAS, 326, L37